

Polyhedral colloidal ‘rocks’: low-dimensional networks

Rebecca Rice¹, Roland Roth² and C. Patrick Royall¹

¹*School of Chemistry, University of Bristol, Bristol, BS8 1TS, UK and*

²*Institut für Theoretische Physik, Universität Erlangen-Nürnberg, Staudtstr. 7, 91058 Erlangen, Germany.*

(Dated: 26th May 2022)

We introduce a model system of anisotropic colloidal ‘rocks’. Due to their shape, the bonding introduced via non-absorbing polymers is profoundly different from spherical particles: bonds between rocks are rigid against rotation, leading to strong frustration. We develop a geometric model which captures the essence of the rocks. Experiments and simulations show that the colloid geometry leads to structures of low fractal dimension. This is in stark contrast to gels of spheres, whose rigidity results from locally dense regions. At high density the rocks form a quasi one-component glass.

PACS numbers: 82.70.Dd;64.60.Cn

Dispersions of mesoscopic colloidal particles are important for several reasons. They model atomic and molecular systems, yet single particle level imaging reveals local phenomena, such as pinpointing mechanisms of dynamic arrest [1, 2], which are inaccessible in conventional systems. Furthermore, colloidal and nanoparticle systems are important materials. Colloidal gels stabilize a range of industrial and consumer products from pesticides to cosmetics. Underlying both is the tuneability of interactions between colloids which are theoretically well understood and hence enable design of self-assembled structures at small lengthscales. Recently, anisotropic interactions using a number of sticky patches per particle have been introduced, opening new routes of self-assembly. Reducing the number of patches per particle leads to networks of low fractal dimension [3].

Here we consider depletion induced gels of anisotropic particles. The addition of polymer mediates an effective attraction between the colloids due to excluded volume effects – see Fig 1(b). The depth of this attraction is proportional to the polymer concentration c_p and the range is set by the polymer size. At sufficient strengths of the depletion attraction, spinodal phase separation leads to colloid-rich (polymer-poor) ‘colloidal liquid’ and colloid-poor (polymer-rich) ‘colloidal gas’ phases. Decreasing the range of the depletion interaction by reducing the size of the polymer relative to the colloid leads to a higher density colloidal liquid. If the packing fraction of the colloidal liquid is high enough ($\phi \approx 0.58$) phase separation is arrested. The resulting network of voids combined with ‘arms’ of high local colloid density, is termed a gel [4].

A range of anisotropic particles has been synthesized [5, 6], and systems with hard interactions have received considerable attention very recently: rods form the expected liquid crystalline phases [7], anisotropy suppresses long-ranged order close to a wall [8] and at high density, colloidal dumbbells show multiple relaxation pathways [9]. However, although networks of anisotropic particles are important, e.g. in shiny paper coatings, systematic experimental studies of the effect of anisotropy in systems with attractions are limited: attractions between colloidal platelets can lead to stacking [10, 11], gels of colloidal rods form bundles [12] and due to their patchy

interactions, clay platelets form low density colloidal ‘liquids’ [13].

Here we introduce an anisotropic colloidal system of faceted polyhedra, or ‘rocks’, with tuneable interactions, amenable to 3D single-particle level analysis with confocal microscopy. Unlike gels of spherical particles where phase separation is suppressed by slow dynamics due to the high local colloid density of the ‘arms’, we show that the polyhedral nature of the rocks leads to bonds which do not rotate and thus rigid structures and networks of low fractal dimension are formed. It appears that for this geometry, a modest depletion attraction can drive the system into a regime similar to diffusion-limited cluster aggregation (DLCA) where the bonding is irreversible. Inspired by the remarkable effect of particle geometry, we develop a model which captures the essential geometrical properties of the colloidal rocks in the form of dodecahedral clusters of 20 spheres, as shown in Fig. 1(e). We further explore the effect of particle geometry at high density and find that the colloidal rocks are a quasi one-component glass-former.

I. EXPERIMENTAL

Faceted polytetrahedral rock-shaped particles as shown in Fig. 1(a) were produced by modifying a synthesis to produce poly-methyl-methacrylate (PMMA) colloids stabilised with poly-hydroxy stearic acid [14]. Details of the synthesis will be presented elsewhere. The particle size is expressed as $\sigma_r = 3.5 \mu\text{m}$, the longest dimension of each rock in images such as Fig. 1(a). It is hard to determine the polydispersity for these particles, which have both shape and some size polydispersity. However, inspection of SEM images suggests that the size polydispersity is $\sim 5\%$. The colloidal rocks were labelled with rhodamine iso-thiocyanate fluorescent dye. To investigate the change induced by anisotropy we also used spherical PMMA particles, of diameter $\sigma_s = 2.4 \mu\text{m}$ with 4% polydispersity determined by static light scattering.

The colloids were dispersed in a density- and refractive index matching mixture of cis-decalin and cyclohexyl bromide (CHB), to which was added 4 mMol of tetrabutyl

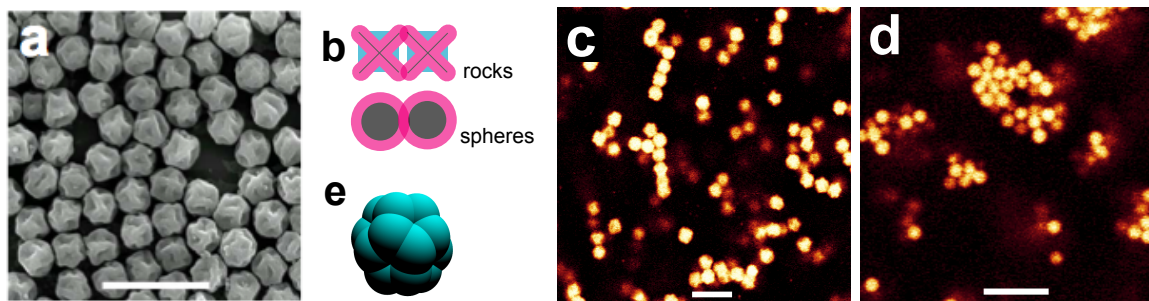


Figure 1: (color online) (a) SEM image of colloidal rocks. (b) Schematic of the mechanism of rigid bonding induced by multiple overlap zones in the rocks contrasted with spheres which are free to rotate. Regions from which the polymer coil center of mass is excluded are shown in pink. (c) Confocal image of a gel of rocks $c_p/c_p^{gel} = 1.13$. (d) Confocal image of a gel of spheres $c_p/c_p^{gel} = 1.44$. c_p is polymer concentration and c_p^{gel} is at the onset of gelation, see Fig. 2. (e) Dodecahedral assembly of 20 spheres used in simulations. Scale bars in a,c,d are 10 μm .

ammonium bromide salt to screen electrostatic interactions [2]. Polystyrene polymer was added to induce depletion attractions. The polymer used was $M_w = 2.1 \times 10^7$ g/mo in the case of the rocks and $M_w = 3.1 \times 10^7$ g/mol for the spheres resulting in polymer radii of gyration of $R_g = 180$ nm and $R_g = 220$ nm [15] and a polymer-colloid size ratio $2R_g/\sigma$ of 0.11 and 0.18, respectively. With the exception of the modest change in interaction range, the experimental conditions were identical for both rocks (r) and spheres (s). The colloid volume fraction $\phi_r = \phi_s = 0.05$ was determined by weighing out the samples. We track the colloid coordinates in 3D using confocal microscopy images. The rocks are sufficiently large with an intensity maximum at the centre of the particle that algorithms developed for spheres [16] identify the rock centres effectively with an error $\lesssim 100$ nm. Particles were defined as bonded if their centres lay within the interaction range $\sigma + 2R_g$, i.e. $3.9 \mu\text{m}$ and $2.8 \mu\text{m}$ for the rocks and spheres respectively. Moderate changes in this bond length had no significant impact on our results.

II. RESULTS AND DISCUSSION

Geometry introduces two key differences between the rocks and spheres relevant to depletion attractions as indicated in Fig. 1(b). Firstly, for rocks the overlap of excluded volume, which drives the depletion interaction, is much reduced compared to spheres. This is due to the concave shape of the rocks which means that much of the volume from which the polymers are excluded cannot overlap due to the approach of two rocks. This is shown by the pink regions in Fig. 1(b) which denote excluded volume, while the black is the colloidal particle. Blue denotes regions where overlap of excluded volume is prevented due to the concave faces. Thus we expect that more polymer is required in the case of the rocks, for a given degree of attraction. Secondly, the faces of the rocks lead to multiple overlap zones as shown by the overlapping pink regions in Fig. 1(b). These impose an

energetic penalty to rotation, which is absent in the case of spheres. Both points were confirmed by calculations with model rocks and ideal polymer.

Confocal microscopy images of gels of rocks and spheres are shown in Fig. 1(c) and (d). The difference is striking: rocks form one-particle wide chains while spheres form densely packed structures. This provides direct evidence for a different bonding scenario in the two species, as indicated in Fig. 1(b). We identify gelation with a percolating network of long-lived bonds. Gel dynamics are shown in supplementary movie 1. In finite sized microscope images, it can be hard to directly measure percolation. We therefore determine percolation through the ratio L_c/L as shown in Fig 2(a), where L_c is the length of the largest connected cluster and L is the image size. Gelation is thus identified with a rapid rise in the ratio L_c/L . The polymer *mass* fraction for gelation c_p^{gel} in the case of spheres is $4.1 \pm 0.5 \times 10^{-4}$ and $2.0 \pm 0.3 \times 10^{-3}$ for the rocks, which corresponds to a *volume* fraction ϕ_p^{gel} of 0.42 ± 0.05 for the spheres and 2.3 ± 0.2 for the rocks. Here the polymer volume fraction is defined $\phi_p = 4\pi\rho_p R_g^3/4$ where ρ_p is polymer number density. We attribute this fivefold change in polymer volume fraction required for gelation to the much reduced overlap volume in the case of the rocks. Effects due to different polymer-colloid size ratios and polymer non-ideality were estimated to be small [17].

The difference between the rocks and spheres in the structure at the particle level is also striking, as shown by the radial distribution functions in Fig. 3(a) and (b). Data for spheres has been compared against computer simulation for hard spheres in [15], showing excellent agreement. The rocks show similar behaviour, indicating that the colloids are stable against aggregation. At higher polymer concentration, although both species show a strong increase in the first peak upon gelation, in the case of spheres, the onset of gelation ($c_p/c_p^{gel} \geq 1$) coincides with $g(r) > 1$ for $r < 5\sigma_s$, indicating clustering/dense regions in agreement with Fig. 1(d). This behaviour is entirely absent in the case of the rocks [Fig.

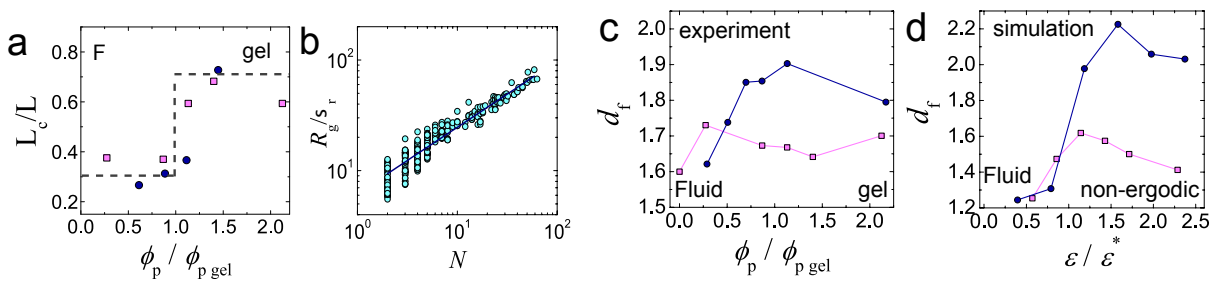


Figure 2: (color online) Percolation and fractal dimension. (a) Size of largest connected region L_c scaled by image size L . Dashed line is a guide to the eye. (b) Radius of gyration of clusters as a function of the number of particles in the cluster plotted to yield the fractal dimension d_f (experimental data from rocks). d_f in experiments (c) and in simulations (d) for isolated clusters with $\phi_r = \phi_s = 0.0125$. In (a,c,d) the rocks are denoted by pink squares \square and the spheres by circles \bullet .

1(c)]. In other words, for spheres, phase separation has already begun before gelation sets in: gelation is driven by the arrest due to the development of the dense phase [4], once it has formed on a lengthscale of several particles. The rocks show no signs of locally dense regions: gelation is driven solely by rigid bonds. Similar conclusions may be reached by considering the number of neighbours of a given particle [Fig. 3(c,d)]. In the case of spheres, the onset of phase separation (gelation) leads to a considerable change in the number of neighbours, indicating locally dense regions. Rocks on the other hand show no such indication of phase separation. In other words, rocks have a reduced valency induced by their geometry with some similarity to patchy particles [3].

This bonding and local structure has significant implications for the network formation. To quantify the structure, we use a local ‘fractal dimension’, d_f , for finite assemblies of particles, which is defined as $R_g^c \propto N^{1/d_f}$ where R_g^c is the radius of gyration of a connected region of N particles, as shown in Fig. 2(b). At the low packing fractions we consider, the fluid phase forms clusters, whose d_f is found in the same way. We plot the resulting d_f in Fig. 2(c). Spheres and rocks show an increase in d_f upon increasing the polymer concentration, up to gelation, after which non-ergodicity leads to a failure to relax locally and a decrease in d_f , as found previously [18]. However, the fractal dimension of rock clusters and gels is significantly lower than that of spheres. This is consistent with the idea that the sphere-based clusters have already begun to condense (leading to an increase in d_f), while the rock clusters show no signs of such condensation. We note that for the rock gels, the measured fractal dimension is even less than that expected for DLCA where $d_f = 1.8$. This is surprising: DLCA assumes unbreakable bonds, which is entirely different from the weak depletion-induced gelation expected in colloid-polymer mixtures.

We have argued that the only relevant difference between the rocks and spheres lies in their shapes and now enquire as to the geometrical origins of the rock behaviour. Unlike other approaches to produce networks with low fractal dimension which rely on a few sticky

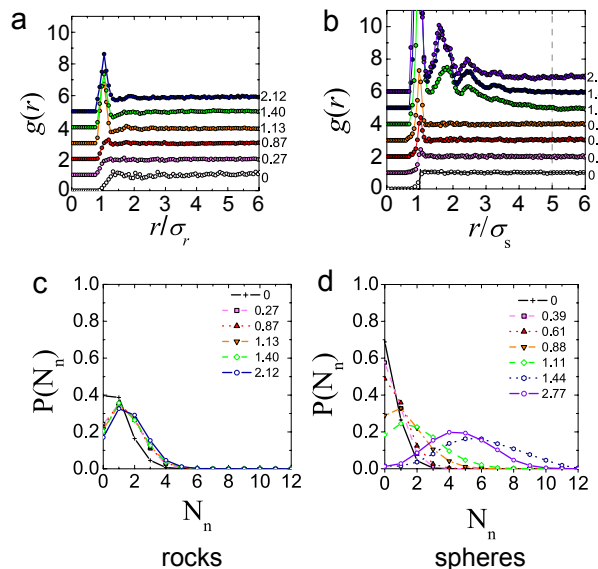


Figure 3: (color online) Radial distribution functions $g(r)$ for rocks (a) and spheres (b), respectively. Dashed line in (b) denotes the approximate lengthscale of incipient phase separation for the spheres. Data are shifted for clarity. Distributions of the number of neighbours $P(N_n)$ for rocks (c) and spheres (d), respectively. Labels denote c_p/c_p^{gel} .

patches on each particle to reduce the number of bonds [3], here we consider only the particle geometry with no restriction on the number of neighbours a particle can have, except the steric limitation which also applies to particle with a spherically symmetric interaction. We introduce a model based on dodecahedral assemblies of 20 overlapping spheres whose centres lie on a sphere, as shown in Fig. 1(e). This model was chosen as a simple representation of the rock shape, as it is reasonably resistant to ordered packing, and the faces should mimic the rigid bonding of the rocks. These (small) spheres have a diameter of $2/7\sigma_c$, where σ_c is the diameter of the circumscribed sphere. The volume of a set of overlapping spheres can be calculated exactly by e.g. the Connolly

algorithm [19] and is approximately $0.416 \sigma_c^3$ for these model rocks.

For short ranged attractions, the detailed form of the interaction potential is irrelevant for many properties [20], so we treat the attractions that result from the addition of polymer with a square well of width $0.042\sigma_c$ and depth ε . We also carry out simulations of spheres of diameter σ_s interacting via the square well potential of width $0.042\sigma_s$. Using the extended law of corresponding states, [20], this maps to a polymer-colloid size ratio of 1/7, comparable to the experiments. Here we focus on the geometric properties, rather than the dynamics: our purpose is to demonstrate the qualitatively different nature of aggregation of spheres and rocks. We therefore use Monte Carlo (MC) simulations in the canonical ensemble with 512 particles. Simulations with more (2048) particles showed minimal differences, as for the state points we consider. We use a short (0.04σ) and long (σ) translational step for both spheres and rocks. The former enables local restructuring of bonded particles, the latter accelerates aggregation. For the rocks, small (0.01 rad) and large (0.2 rad) rotational moves are also used. Each simulation is ‘equilibrated’ for 10^4 MC sweeps prior to sampling. Each sweep involves attempted moves of all types. Simulations are repeated at least six times.

In Fig. 2(d) we plot fractal dimensions for simulations of rocks and spheres for packing fraction $\phi_r = \phi_s = 0.0125$ (the experiments are carried out at $\phi_r = \phi_s = 0.05$) [21]. The spheres exhibit similar behaviour as in the experiments, with $d_f \sim 2$ when the system falls out of equilibrium on the simulation timescale. This we take as the strength of attraction associated with spinodal decomposition [4], which corresponds to $\beta\varepsilon^* \approx 2.53$, noting that for such short-ranged interactions, the spinodal line depends rather weakly on ϕ . For the rocks, we identify $\varepsilon^* \approx 1.75 k_B T$ with the onset of a regime where the potential energy decreases continuously. Both rock and sphere d_f are lower than the experiments at low attraction, which may be related to the change in ϕ .

The simulations clearly show that the rock clusters have a fractal dimension which is less than that of the spheres [Figs. 2(c,d)]. In fact $d_f \approx 1.5$, even less than in the experiments. Although the simulation results are presented for a lower density the agreement between experiment and simulation adds further weight to our hypothesis that (i) the rocks have an intrinsically different bonding mechanism compared to spheres driven by geometry and (ii) that their behaviour is qualitatively captured by the dodecahedral clusters. Since the rocks can bond to as many neighbours as they have faces, they can form dense phases and therefore, at equilibrium dense and dilute phases coexist so the rock gels should be metastable.

The fractal dimension of rock clusters, both in experiments with percolating networks and simulations of isolated clusters is low, ~ 1.7 and ~ 1.5 respectively, lower even than DLCA. Cates *et.al.* [22], suggested that sim-

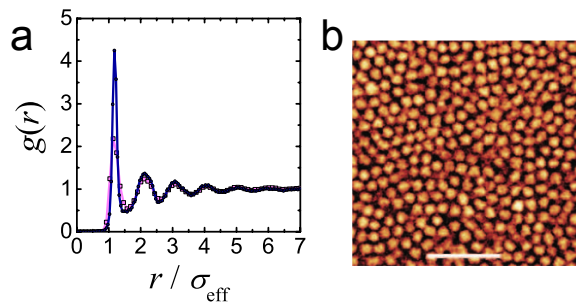


Figure 4: (color online) (a) Mapping $g(r)$ of rocks at $\phi_r = 0.48$ (pink squares) and $g(r)$ of spheres at $\phi_s = 0.54$ (black circles) from experiments. σ_{eff} denotes σ_r and σ_s for rocks and spheres respectively. We estimate the mapping by comparing the higher-order peaks. At the time of measurement the metastable sphere fluid showed no signs of crystallisation. (b) Confocal image of rock glassy state. Bar=10 μm .

ilar behaviour might be found in spheres, if they were suddenly – and deeply – quenched to the regime where DLCA dominates. The rock geometry may be interpreted as exhibiting similar behaviour with much weaker attractions.

Finally, we consider the high density behaviour. In experiments without polymer, rocks did not crystallise at a packing fraction $\phi_r = 0.46$ on a timescale of one week (Fig. 4). This is reasonable, as it has recently been shown that only a limited degree of asphericity is required to suppress crystallisation [23]. Supplementary movie 2 shows that rocks at $\phi_r = 0.46$ exhibit glassy dynamics, with displacement hindered by their neighbours. We find that the radial distribution function of dense amorphous packings of rocks at $\phi_r = 0.46$ has peak locations and a decay of the oscillations similar to the $g(r)$ of spheres at $\phi_s = 0.54$ [Fig. 4(a)]. This indicates that the longer-range structure is similar, suggesting an effective packing fraction for the rocks higher than $\phi_r = 0.46$, likely due to the concave geometry. The failure of the rocks to crystallise indicates that they are a ‘quasi one-component glass former’.

III. CONCLUSIONS

We have developed an experimental model system of anisotropic colloidal rocks whose interactions can be tuned and which can be visualized directly in 3D. Due to their shape, the bonding introduced via the depletion attraction is profoundly different to spheres: the bonds formed between rocks are rigid against particle rotation. The frustration induced by this change in geometry profoundly influences the kinetic pathway: rocks form open networks of low fractal dimension. We presume that the rock gels are, like gels of spheres, ultimately metastable to phase separation, but expect that the rock gels should be very long-lived. We demonstrated that geometry is the dominant driver for this behaviour by intro-

ducing a model of dodecahedral clusters which captures the essence of the colloidal rocks. At higher density the experimental system forms a quasi-one-component glass.

Our work opens up a single particle level approach to tackle important problems such as the role of friction and surface roughness in colloidal and nanoparticle processing and jamming. We hope to stimulate further experiments, for example the use of external fields such as shear, along with theoretical and simulation work which may fully determine the phase diagram, and the role of particle geometry in kinetic trapping and its interplay

with hydrodynamic interactions. Self assembly of nanodevices requires avoidance of kinetic trapping [24]; here we have shown the potential of direct visualisation as a means to develop control of self-assembly which may yield insight into nano-assembly.

Acknowledgments R. Rice and CPR gratefully acknowledge the Royal Society for financial support. The authors would like to thank Doug Ashton, Paul Bartlett, Patrick Charbonneau, Bob Evans, Rob Jack and John Russo for helpful discussions.

-
- [1] E. Weeks, J. Crocker, A. Levitt, A. Schofield, and D. Weitz, *Science* **287**, 627 (2001).
 - [2] C. P. Royall, S. R. Williams, T. Ohtsuka, and H. Tanaka, *Nature Mater.* **7**, 556 (2008).
 - [3] E. Bianchi, J. Largo, P. Tartaglia, E. Zaccarelli, and F. Sciortino, *Phys. Rev. Lett.* **97**, 168301 (2006).
 - [4] P. J. Lu, E. Zaccarelli, F. Ciulla, A. B. Schofield, F. Sciortino, and D. A. Weitz, *Nature* **435**, 499 (2008).
 - [5] S. C. Glotzer and M. J. Solomon, *Nature Materials* **6**, 557 (2007).
 - [6] D. J. Kraft, J. Groenewold, and W. K. Kegel, *Soft Matter* **5**, 3823 (2009).
 - [7] A. Kuijk, A. van Blaaderen, and A. Imhof, *J. Am. Chem. Soc.* **133**, 2346 (2011).
 - [8] R. P. A. Dullens, M. C. D. Mourad, D. G. A. L. Aarts, J. P. Hoogenboom, and W. K. Kegel, *Phys. Rev. Lett.* **96**, 028304 (2006).
 - [9] R. C. Kramb, R. Zhang, K. S. Schweizer, and C. F. Zukoski, *Phys. Rev. Lett.* **105**, 055702 (2010).
 - [10] M. Zhao and T. G. Mason, *Phys. Rev. Lett.* **99**, 268301 (2007).
 - [11] Z. Zhang, P. Pfeiderer, A. B. Schofield, C. Clasen, and J. Vermant, *J. Am. Chem. Soc.* **133**, 392 (2011).
 - [12] G. M. H. Wilkins, P. T. Spicer, and M. J. Solomon, *Langmuir* **25**, 8951 (2009).
 - [13] B. Ruzicka, E. Zaccarelli, L. Zulian, R. Angelini, M. Sz-tucki, A. Moussaid, T. Narayanan, and F. Sciortino, *Nature Materials* **10**, 56 (2010).
 - [14] R. P. A. Dullens, M. Claesson, D. Derks, A. van Blaaderen, and W. K. Kegel, *Langmuir* **19**, 5963 (2003).
 - [15] C. P. Royall, A. A. Louis, and H. Tanaka, *J. Chem. Phys.* **127**, 044507 (pages 8) (2007).
 - [16] C. P. Royall, M. Leunissen, and A. van Blaaderen, *J. Phys: Condens. Matter* **15**, 3581 (2003).
 - [17] A. A. Louis, P. G. Bolhuis, E. J. Meijer, and J. P. Hansen, *J. Chem. Phys.* **117**, 1893 (2002).
 - [18] T. Ohtsuka, C. P. Royall, and H. Tanaka, *Europhys. Lett.* **84**, 46002 (2008).
 - [19] M. Connolly, *J. Am. Chem. Soc.* **107**, 1118 (1985).
 - [20] M. G. Noro and D. Frenkel, *J. Chem. Phys.* **113**, 2941 (2000).
 - [21] The simulations are carried out at a lower packing fraction to avoid the effects of percolation which limit the statistics gathered in our calculation of $\langle df \rangle$.
 - [22] M. Cates, M. Fuchs, W. C. K. Kroy, K. Poon, and A. M. Puertas, *J. Phys. Condens* **16**, S4861 (2004).
 - [23] W. L. Miller, B. Bozorgui, and A. Cacciuto, *J. Chem. Phys.* **13**, 234903 (2010).
 - [24] G. M. Whitesides and M. Boncheva, *Proc. Nat. Acad. Sci.* **99**, 4769 (2002).